Author(s): Tuovinen, Toni & Hinkkanen, Marko & Luomi, Jorma

Title: Analysis and design of a position observer with resistance adaptation for synchronous reluctance motor drives

Year: 2011

Version: Post print

Please cite the original version:

Tuovinen, Toni & Hinkkanen, Marko & Luomi, Jorma. 2011. Analysis and design of a position observer with resistance adaptation for synchronous reluctance motor drives. 2011 IEEE Energy Conversion Congress and Exposition (ECCE). 8. ISBN 978-1-4577-0542-7 (electronic). DOI: 10.1109/ecce.2011.6063753.

Analysis and Design of a Position Observer with Resistance Adaptation for Synchronous Reluctance Motor Drives

Toni Tuovinen, Marko Hinkkanen, and Jorma Luomi

Aalto University School of Electrical Engineering
Department of Electrical Engineering, P.O. Box 13000, FI-00076 Aalto, Finland

***Abstract*—A back-EMF-based reduced-order position observer with stator-resistance adaptation is analyzed for motion-sensorless synchronous reluctance motor drives. Analytical equations for steady-state estimation errors and stability conditions are derived (with and without resistance adaptation), taking into account errors in the parameter estimates. The effect of the observer gain on the noise reduction is studied by means of eigenvector analysis. A robust gain selection is proposed, which maximizes the allowed uncertainties in the parameter estimates. The proposed observer design is experimentally evaluated using a 6.7-kW synchronous reluctance motor drive; stable operation is demonstrated at low speeds under various parameter errors.**

***Index Terms*—Observer, stability conditions, speed sensorless, stator resistance estimation.**

I. Introduction

Modern synchronous reluctance motors (SyRMs) are becoming interesting competitors to induction motors and permanent-magnet synchronous motors in variable-speed drives [1], [2]. The rotor position of a synchronous motor has to be known with good accuracy in order to obtain stable operation and high performance. The rotor position can be either measured or estimated. Motion-sensorless control is usually preferable: motion sensors are expensive, they can be damaged or, in some environments and applications, cannot be installed.

Signal-injection-based methods can be used for SyRMs. In order to avoid additional noise and losses, it is desirable to use a method based on the back electromotive force (EMF), and combine a signal-injection method with it only at the lowest speeds [3], [4]. Back-EMF-based observers for SyRM drives have been proposed in [1], [5]–[8]. However, the stability analysis has been omitted, with the exception of [8]. The effect of parameter uncertainties should be accounted for in the stability analysis, which makes the task even more complicated. The model parameters are rarely known accurately, and in practice, they are not constant. The stator resistance varies with the winding temperature during the operation of the motor. The d-axis flux component usually saturates strongly as a function of the d-axis current component, and the d-axis saturation is coupled with the q-axis saturation [9].

In this paper, a reduced-order observer with stator-resistance adaptation—originally proposed for PMSM drives in [10]—is applied for SyRM drives. Analytical equations for steady-state estimation errors and stability conditions are derived, taking into account errors in the parameter estimates (that were omitted in the analysis in [10]). Based on these design tools, a robust gain selection is proposed, which maximizes the allowed uncertainties in the parameter estimates. Furthermore, the effect of the observer gain on the noise reduction is studied by means of eigenvector analysis. If desired, the observer could be augmented with a signal-injection method, for example in a fashion similar to [3]. The performance of the proposed observer design is evaluated using laboratory experiments with a 6.7-kW SyRM drive.

II. SyRM Model and Rotor-Position Observer

A. Model

Real space vectors will be used here. For example, the stator-current vector is $\boldsymbol{i}_\mathrm{s} = [i_\mathrm{d}, i_\mathrm{q}]^\mathrm{T}$, where i_d and i_q are the components of the vector and the matrix transpose is marked with the superscript T. The identity matrix and the orthogonal rotation matrix are defined as

$$\mathbf{I} = \begin{bmatrix} 1 & 0 \\ 0 & 1 \end{bmatrix}, \quad \mathbf{J} = \begin{bmatrix} 0 & -1 \\ 1 & 0 \end{bmatrix}.$$

The electrical position of the d axis is denoted by ϑ_m. The d axis is defined as the direction of the maximum inductance of the rotor. The position depends on the electrical angular rotor speed ω_m according to

$$\frac{\mathrm{d}\vartheta_\mathrm{m}}{\mathrm{d}t} = \omega_\mathrm{m} \tag{1a}$$

To simplify the analysis in the following sections, the machine model will be expressed in the *estimated* rotor reference frame, whose d axis is aligned at $\hat{\vartheta}_\mathrm{m}$ with respect to the stator reference frame. The stator inductance is

$$\boldsymbol{L} = \mathrm{e}^{-\tilde{\vartheta}_\mathrm{m}\mathbf{J}} \begin{bmatrix} L_\mathrm{d} & 0 \\ 0 & L_\mathrm{q} \end{bmatrix} \mathrm{e}^{\tilde{\vartheta}_\mathrm{m}\mathbf{J}} \tag{1b}$$

where $\tilde{\vartheta}_\mathrm{m} = \hat{\vartheta}_\mathrm{m} - \vartheta_\mathrm{m}$ is the estimation error in the rotor position, L_d the direct-axis inductance, and L_q the quadrature-axis inductance. The voltage equation is

$$\frac{\mathrm{d}\boldsymbol{\psi}_\mathrm{s}}{\mathrm{d}t} = \boldsymbol{u}_\mathrm{s} - R_\mathrm{s}\boldsymbol{i}_\mathrm{s} - \hat{\omega}_\mathrm{m}\mathbf{J}\boldsymbol{\psi}_\mathrm{s} \tag{1c}$$

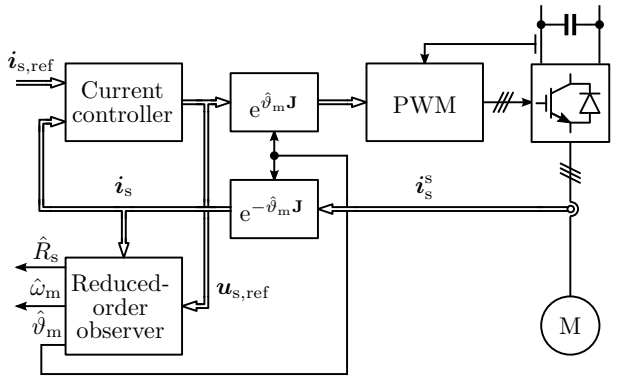

Fig. 1. Motion-sensorless rotor-oriented controller. The observer is implemented in the estimated rotor coordinates.

where $\boldsymbol{\psi}_\mathrm{s}$ is the stator-flux vector, $\boldsymbol{u}_\mathrm{s}$ the stator-voltage vector, R_s the stator resistance, and $\hat{\omega}_\mathrm{m} = \mathrm{d}\hat{\vartheta}_\mathrm{m}/\mathrm{d}t$ is the angular speed of the coordinate system. The stator current is a nonlinear function

$$\boldsymbol{i}_\mathrm{s} = \boldsymbol{L}^{-1}\boldsymbol{\psi}_\mathrm{s} \tag{1d}$$

of the stator-flux vector and the position error $\tilde{\vartheta}_\mathrm{m}$.

B. Observer

A typical rotor-oriented control system is depicted in Fig. 1, where the reduced-order observer proposed in [10] is considered. It is based on estimating the rotor position and the d component $\hat{\psi}_\mathrm{d}$ of the stator flux in estimated rotor coordinates. For a SyRM, the componentwise presentation of the observer is

$$\frac{\mathrm{d}\hat{\psi}_\mathrm{d}}{\mathrm{d}t} = u_\mathrm{d} - \hat{R}_\mathrm{s} i_\mathrm{d} + \hat{\omega}_\mathrm{m}\hat{L}_\mathrm{q} i_\mathrm{q} + k_1(\hat{\psi}_\mathrm{d} - \hat{L}_\mathrm{d} i_\mathrm{d}) \tag{2a}$$

$$\frac{\mathrm{d}\hat{\vartheta}_\mathrm{m}}{\mathrm{d}t} = \frac{u_\mathrm{q} - \hat{R}_\mathrm{s} i_\mathrm{q} - \hat{L}_\mathrm{q}\frac{\mathrm{d}i_\mathrm{q}}{\mathrm{d}t} + k_2(\hat{\psi}_\mathrm{d} - \hat{L}_\mathrm{d} i_\mathrm{d})}{\hat{\psi}_\mathrm{d}} \tag{2b}$$

where $\hat{R}_\mathrm{s}$, $\hat{L}_\mathrm{d}$ and $\hat{L}_\mathrm{q}$ are estimates of the corresponding actual parameters, and k_1 and k_2 are observer gains. The observer is of the second order and there are only two gains.

With accurate parameter estimates, the closed-loop system consisting of (1) and (2) is locally stable in every operating point if the gains are given by

$$k_1 = -\frac{b + \beta(c/\hat{\omega}_\mathrm{m} - \hat{\omega}_\mathrm{m})}{\beta^2 + 1}, \quad k_2 = \frac{\beta b - c/\hat{\omega}_\mathrm{m} + \hat{\omega}_\mathrm{m}}{\beta^2 + 1} \tag{3}$$

where $\beta = i_\mathrm{q}/i_\mathrm{d}$ and the design parameters $b > 0$ and $c > 0$ may depend on the operating point[1]. The observer gain design problem is reduced to the selection of the two positive parameters b and c, which are actually the coefficients of the characteristic polynomial of the linearized closed-loop system. Hence, (3) can be used to place the poles of the linearized closed-loop system arbitrarily.

[1]For $\hat{\omega}_\mathrm{m} = 0$, $c = 0$ has to be selected to avoid division by zero, giving only marginal stability for zero speed.

For improved robustness at the lowest speeds, the observer (2) can be augmented with the stator-resistance adaptation law [10]

$$\frac{\mathrm{d}\hat{R}_\mathrm{s}}{\mathrm{d}t} = k_\mathrm{R}(\hat{\psi}_\mathrm{d} - \hat{L}_\mathrm{d} i_\mathrm{d}) \tag{4}$$

where k_R is the adaptation gain. With accurate parameter estimates, the general stability conditions for the system augmented with (4) are

$$k_\mathrm{R} i_\mathrm{q}\hat{\omega}_\mathrm{m} > 0 \tag{5a}$$

$$k_\mathrm{R}[(i_\mathrm{d} - \beta i_\mathrm{q})b - 2i_\mathrm{q}\hat{\omega}_\mathrm{m}] + bc > 0 \tag{5b}$$

where b and c are the positive design parameters in (3).

III. Selection of Gains

With parameter errors included, the stability is not guaranteed for all positive values of the design parameters b and c in (3). It will be studied how these design parameters should be chosen in order to reduce sensitivity to parameter errors (Section III-A) and process noise (Section III-B).

The nonlinear estimation error dynamics of the closed-loop system consisting of (1) and (2) are

$$\frac{\mathrm{d}\tilde{\boldsymbol{\psi}}_\mathrm{s}}{\mathrm{d}t} = (\boldsymbol{K}\hat{\boldsymbol{L}}^{-1} - \hat{\omega}_\mathrm{m}\mathbf{J})\tilde{\boldsymbol{\psi}}_\mathrm{s} + \left[\boldsymbol{K}(\hat{\boldsymbol{L}}^{-1}\boldsymbol{L} - \mathbf{I}) - \tilde{R}_\mathrm{s}\right]\boldsymbol{i}_\mathrm{s} \tag{6a}$$

where the gain matrix is

$$\boldsymbol{K} = \begin{bmatrix} k_1\hat{L}_\mathrm{d} & 0 \\ k_2\hat{L}_\mathrm{d} & 0 \end{bmatrix}. \tag{6b}$$

The estimation error of the stator flux is $\tilde{\boldsymbol{\psi}}_\mathrm{s} = \hat{\boldsymbol{\psi}}_\mathrm{s} - \boldsymbol{\psi}_\mathrm{s}$ and other estimation errors are defined similarly. In the reduced-order observer (2), the error of the q-axis flux is a nonlinear function of the position error, since $\hat{\psi}_\mathrm{q} = \hat{L}_\mathrm{q} i_\mathrm{q}$ and

$$\begin{aligned}\psi_\mathrm{q} =& \frac{1}{2}(L_\mathrm{q} - L_\mathrm{d})\left(\sin(2\tilde{\vartheta}_\mathrm{m})i_\mathrm{d} + \cos(2\tilde{\vartheta}_\mathrm{m})i_\mathrm{q}\right) \\ &+ \frac{1}{2}(L_\mathrm{d} + L_\mathrm{q})i_\mathrm{q}.\end{aligned} \tag{6c}$$

A. Stability With Uncertain Parameters

With erroneous parameter estimates, the stability of (6) should be analyzed in the vicinity of the steady-state position error $\tilde{\vartheta}_{\mathrm{m}0}$ that is nonzero. It is assumed that the estimation error consists of the steady-state error and a small variation in the vicinity of that steady-state error. In steady-state, the time derivative of $\tilde{\boldsymbol{\psi}}_\mathrm{s}$ in (6) vanishes. The equation for the steady-state position error $\tilde{\vartheta}_{\mathrm{m}0}$ is

$$A\cos 2\tilde{\vartheta}_{\mathrm{m}0} + B\sin 2\tilde{\vartheta}_{\mathrm{m}0} + C = 0 \tag{7a}$$

where

$$A = -\hat{\omega}_\mathrm{m}(L_\mathrm{d} - L_\mathrm{q})\left[k_1 + \beta(\hat{\omega}_\mathrm{m} - k_2)\right] \tag{7b}$$

$$B = -\hat{\omega}_\mathrm{m}(L_\mathrm{d} - L_\mathrm{q})\left[(\hat{\omega}_\mathrm{m} - k_2) - \beta k_1\right] \tag{7c}$$

$$\begin{aligned}C =& \left[(2\hat{L}_\mathrm{d} - L_\mathrm{d} - L_\mathrm{q})k_1\hat{\omega}_\mathrm{m} + 2\tilde{R}_\mathrm{s}(\hat{\omega}_\mathrm{m} - k_2)\right] \\ &+ \left[2\tilde{R}_\mathrm{s}k_1 + \hat{\omega}_\mathrm{m}(L_\mathrm{d} + L_\mathrm{q} - 2\hat{L}_\mathrm{q})(\hat{\omega}_\mathrm{m} - k_2)\right]\beta.\end{aligned} \tag{7d}$$

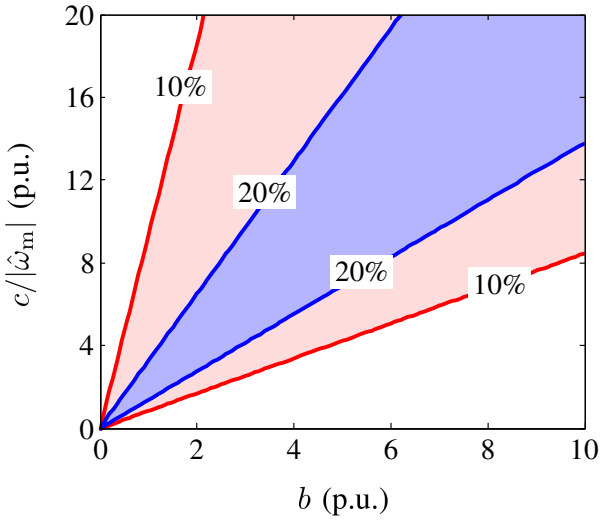

Fig. 2. Stability map in the design parameter space. All $b > 0$ and $c > 0$ guarantee stable operation with the accurate parameter estimates. The operating point corresponds to $\hat{\omega}_\mathrm{m} = 0.05$ p.u., $i_\mathrm{d} = 0.4$ p.u., $i_\mathrm{q} = 0$. The worst-case stability boundaries corresponding to the parameter uncertainties of 10% and 20% are shown by solid lines.

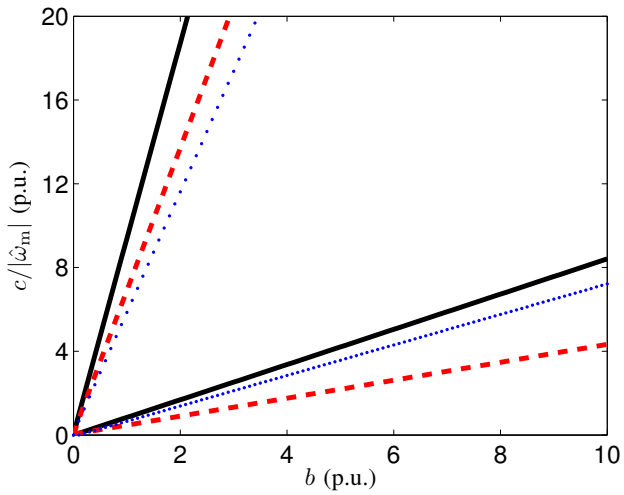

Fig. 3. Areas of stable operation for three different values of i_q for the parameter uncertainties of 10% and $\hat{\omega}_\mathrm{m} = 0.05$ p.u.: i_q = 0 p.u. (solid line), i_q = 0.8 p.u. (dotted line), and i_q = −0.8 p.u. (dashed line).

The solution for the steady-state position error is

$$\tilde{\vartheta}_\mathrm{m0} = -\frac{\sin^{-1}\left(\frac{C}{D}\right) + \phi}{2} \tag{8a}$$

where

$$\phi = \tan^{-1}\left(\frac{A}{B}\right), \quad D = \frac{B}{\cos\phi} \tag{8b}$$

If the steady-state error of the d axis flux is of interest, it can be obtained from

$$\tilde{\psi}_\mathrm{d0} = \frac{i_\mathrm{q}\left[2\tilde{R}_\mathrm{s} + k_2\sin(2\tilde{\vartheta}_\mathrm{m0})(L_\mathrm{d} - L_\mathrm{q})\right]}{2(k_2 - \hat{\omega}_\mathrm{m})} - \frac{i_\mathrm{d}k_2\left[(L_\mathrm{d} - L_\mathrm{q})\cos(2\tilde{\vartheta}_\mathrm{m0}) + L_\mathrm{d} + L_\mathrm{q} - 2\hat{L}_\mathrm{d}\right]}{2(k_2 - \hat{\omega}_\mathrm{m})} \tag{9}$$

after $\tilde{\vartheta}_\mathrm{m0}$ is solved.

The estimation error dynamics (6) are linearized in the vicinity of this steady-state error $\tilde{\vartheta}_\mathrm{m0}$, yielding

$$\frac{\mathrm{d}}{\mathrm{d}t}\begin{bmatrix}\tilde{\psi}_\mathrm{d}\\ \tilde{\psi}_\mathrm{q}\end{bmatrix} = \begin{bmatrix}k_{10} & -k_{10}\beta' + \omega_\mathrm{m0}\\ k_{20} - \omega_\mathrm{m0} & -k_{20}\beta'\end{bmatrix}\begin{bmatrix}\tilde{\psi}_\mathrm{d}\\ \tilde{\psi}_\mathrm{q}\end{bmatrix} \tag{10a}$$

where

$$\beta' = \tan(2\tilde{\vartheta}_\mathrm{m0} + \tan^{-1}\beta_0) \tag{10b}$$

and operating-point quantities are denoted by the subscript 0. The system (6) is locally stable if

$$b' = k_{20}\beta' - k_{10} > 0 \tag{11a}$$

$$c' = \hat{\omega}_\mathrm{m0}^2 - \hat{\omega}_\mathrm{m0}\left[k_{20} + k_{10}\beta'\right] > 0 \tag{11b}$$

where b' and c' are coefficients of the characteristic polynomial of (10a). With accurate parameter estimates, $\beta' = \tan(\tan^{-1}\beta_0) = \beta$, and (11) leads to (3). Equations (7) and (11) could be used to minimize the steady-state position error, to eliminate the effect of a certain parameter error[2], or to maximize the parameter tolerances.

The conditions (11) are studied in no load operation with actual parameters L_d = 2.50 p.u., L_q = 0.397 p.u., and R_s = 0.043 p.u. of a 6.7-kW SyRM. The same relative uncertainty is assumed for all three parameter estimates $\hat{L}_\mathrm{d}$, $\hat{L}_\mathrm{q}$, and $\hat{R}_\mathrm{s}$. Hence, eight different worst-case combinations, consisting of minimum and maximum values of the parameter estimates, can be formed. For example, if the relative uncertainty is defined to be 20%, one of the worst-case combinations is $\hat{L}_\mathrm{d} = 0.8L_\mathrm{d}$, $\hat{L}_\mathrm{q} = 1.2L_\mathrm{q}$, and $\hat{R}_\mathrm{s} = 0.8R_\mathrm{s}$.

At each studied operating point, the local stability of the observer was analyzed for all eight worst-case combinations of erroneous parameter estimates. First, the estimation error of the rotor position was analytically solved in steady state. Then, the local stability of this operating point was checked using (11).

The stability of the estimation-error dynamics with erroneous parameter estimates was analyzed for different values of the design parameters b and c. Fig. 2 shows an example of the stability map in the design-parameter space for the parameter uncertainties of 10% and 20%. In the figure, the vertical axis is scaled with the inverse rotor speed (in order to help the comparison at different speeds). The operating point in Fig. 2 is defined by $\hat{\omega}_\mathrm{m} = 0.05$ p.u., $i_\mathrm{d} = 0.4$ p.u., and $i_\mathrm{q} = 0$. It can be seen that the region of b and c yielding the stable operation is large even in the case of the parameter uncertainty of 20%. As the parameter uncertainty increases, the stable region shrinks (and disappears if the uncertainty is high enough). The size of the stable region depends on the speed and the current components, but its shape remains approximately unchanged. Based on the analysis results, the

[2]For example, the choice $k_2 = k_1\beta + \hat{\omega}_\mathrm{m}$ eliminates $\tilde{R}_\mathrm{s}$.

design parameter c can be chosen as

$$c = \kappa b|\hat{\omega}_\mathrm{m}| + \hat{\omega}_\mathrm{m}^2 \tag{12}$$

where the parameter κ should approximately correspond to the slope of the line passing through the centers of the stable regions in the stability maps, cf. Fig. 2 as an example. As the uncertainty increases, eventually with the combination $\hat{L}_\mathrm{d} < L_\mathrm{d}$ and $\hat{R}_\mathrm{s} > R_\mathrm{s}$, b' in (11) becomes negative, and with the combination $\hat{L}_\mathrm{d} > L_\mathrm{d}$ and $\hat{R}_\mathrm{s} < R_\mathrm{s}$, $|C/D|$ in (8) is larger than one, suggesting that there is no steady-state solution for that combination. Provided that $b \gg \hat{\omega}_\mathrm{m}$, it can be shown that the largest possible parameter uncertainty is achieved with $\kappa = \sqrt{3}$ for SyRMs.

In Fig. 3, the stability map for the parameter uncertainties of 10% is depicted for three different values of i_q in a fashion similar to Fig. 2. The d axis current is i_d = 0.4 p.u. The values for i_q are -0.8 p.u., 0 and 0.8 p.u., corresponding to the negative rated load, no load and the rated load. It can be seen that the area of stable operation rotates clockwise as $|i_\mathrm{q}|$ increases. It seems that a slightly lower value of κ can be used for generator operation than for no-load operation. This result can be used to reduce noise in generator operation.

B. Noise Reduction

In this subsection, accurate parameters are considered. The eigenvalues of the linearized estimation-error dynamics are

$$s_{1,2} = \frac{-b \pm \sqrt{b^2 - 4c}}{2} \tag{13}$$

At low speeds, $s_1 \approx -\kappa|\hat{\omega}_\mathrm{m}|$ and $s_2 \approx -b + \kappa|\hat{\omega}_\mathrm{m}|$. In multiple-input-multiple-output systems, the eigenvalues do not provide all the necessary information considering the system dynamics. The eigenvalues describe the gains in the directions of the corresponding eigenvectors. In order to reduce the noise in the position estimate, the eigenvectors of (10a) are analyzed in the following, and a modification to (12) is proposed.

Provided that $|s_1| \neq |s_2|$, any value of $\tilde{\boldsymbol{\psi}}_\mathrm{s}$ can be written as $\tilde{\boldsymbol{\psi}}_\mathrm{s} = \lambda_1 \boldsymbol{v}_1 + \lambda_2 \boldsymbol{v}_2$, where $\boldsymbol{v}_1$ and $\boldsymbol{v}_2$ are the eigenvectors corresponding to s_1 and s_2, respectively. The equation for the small-signal dynamics (10a) can be written as

$$\frac{\mathrm{d}\tilde{\boldsymbol{\psi}}_\mathrm{s}}{\mathrm{d}t} = s_1\lambda_1\boldsymbol{v}_1 + s_2\lambda_2\boldsymbol{v}_2 \tag{14}$$

The normalized eigenvectors are

$$\boldsymbol{v}_1 = \frac{-1}{\sqrt{(s_2^2 - \hat{\omega}_\mathrm{m}^2)(1+\beta^2)}} \begin{bmatrix} \beta s_2 - \hat{\omega}_\mathrm{m} \\ s_2 + \beta\hat{\omega}_\mathrm{m} \end{bmatrix} \tag{15a}$$

$$\boldsymbol{v}_2 = \frac{-1}{\sqrt{(s_1^2 - \hat{\omega}_\mathrm{m}^2)(1+\beta^2)}} \begin{bmatrix} \beta s_1 - \hat{\omega}_\mathrm{m} \\ s_1 + \beta\hat{\omega}_\mathrm{m} \end{bmatrix} \tag{15b}$$

If c is smaller than b, which is the case at low speeds, $|s_1|$ is small as compared to $|s_2|$, corresponding to slow and fast dynamics, respectively. It might be desirable that the d axis component of the estimated stator flux is updated in the faster time scale, and the q axis component (angle) is updated in the slower time scale, because the flux dynamics are faster than the speed dynamics. Hence, $\boldsymbol{v}_1$ should point to the q axis direction and $\boldsymbol{v}_2$ should point to the d axis direction, or close to it.

At some operating points, both eigenvectors may point to the q axis direction. Consequently, a small error in the estimated d axis component is compensated by updating the q axis component. Furthermore, the d component of $\boldsymbol{v}_2$ is zero when $\kappa\beta\,\mathrm{sign}(\hat{\omega}_\mathrm{m}) \approx -1$ (since $\beta s_1 \approx -\beta\kappa|\hat{\omega}_\mathrm{m}|$). In the regenerating mode, the eigenvector of the faster time scale points to the q axis direction, which means that the rotor angle is updated in the faster time scale.

The fast eigenvector can be rotated more to the d axis direction by decreasing the value of κ. A lower limit κ_min has to be used for κ since too small values might lead to instability if the parameters are not accurate enough. Therefore, κ in (12) is chosen as

$$\kappa = \begin{cases} \kappa_\mathrm{min}, & \text{if } \sqrt{3} + \beta\,\mathrm{sign}(\hat{\omega}_\mathrm{m}) \leq \kappa_\mathrm{min} \\ \sqrt{3} - |\beta|, & \text{if } \kappa_\mathrm{min} < \sqrt{3} + \beta\,\mathrm{sign}(\hat{\omega}_\mathrm{m}) < \sqrt{3} \\ \sqrt{3}, & \text{otherwise.} \end{cases} \tag{16}$$

It can be seen that the value of κ is decreased in the regenerating mode, and κ is constant in the motor mode and no-load.

The tracks of the normalized eigenvectors as i_q changes are depicted in Fig. 4 in two cases. The eigenvectors corresponding to slow and fast dynamics are depicted for $\kappa = \sqrt{3}$ in Figs. 4(a) and 4(b), respectively. The eigenvectors corresponding to slow and fast dynamics are depicted when κ is selected according to (16) with $\kappa_\mathrm{min} = 0.6$ In Figs. 4(c) and 4(d), respectively. The component i_q changes from -1 p.u. to 1 p.u., b = 5, i_d = 0.4 p.u., and $\hat{\omega}_\mathrm{m}$ = 0.1 p.u.

C. Stator-Resistance Adaptation

The nonlinear estimation error dynamics of the system augmented with stator-resistance adaptation consist of (6) and (4). The steady-state position error $\tilde{\vartheta}_\mathrm{m0}$ is determined by

$$A\cos 2\tilde{\vartheta}_\mathrm{m0} + B\sin 2\tilde{\vartheta}_\mathrm{m0} + C = 0 \tag{17}$$

where

$$A = \left(1-\beta^2\right)\left(L_\mathrm{d} - L_\mathrm{q}\right) \tag{18a}$$

$$B = -2\beta(L_\mathrm{d} - L_\mathrm{q}) \tag{18b}$$

$$C = \left(1+\beta^2\right)\left(L_\mathrm{d} + L_\mathrm{q}\right) - 2\left(\hat{L}_\mathrm{d} + \beta^2\hat{L}_\mathrm{q}\right) \tag{18c}$$

The solution for the steady-state position error is given by (8), unless $|\beta| = 1$ (coefficient A vanishes) or $\beta = 0$ (coefficient B vanishes). If $|\beta| = 1$, the steady-state position error is given by

$$\sin(2\tilde{\vartheta}_\mathrm{m0}) = \mathrm{sign}(\beta)\frac{L_\mathrm{d} - \hat{L}_\mathrm{d} + L_\mathrm{q} - \hat{L}_\mathrm{q}}{L_\mathrm{d} - L_\mathrm{q}} \tag{19}$$

and if $\beta = 0$, the steady-state position error is given by

$$\cos(2\tilde{\vartheta}_\mathrm{m0}) = \frac{2\hat{L}_\mathrm{d} - L_\mathrm{d} - L_\mathrm{q}}{L_\mathrm{d} - L_\mathrm{q}} \tag{20}$$

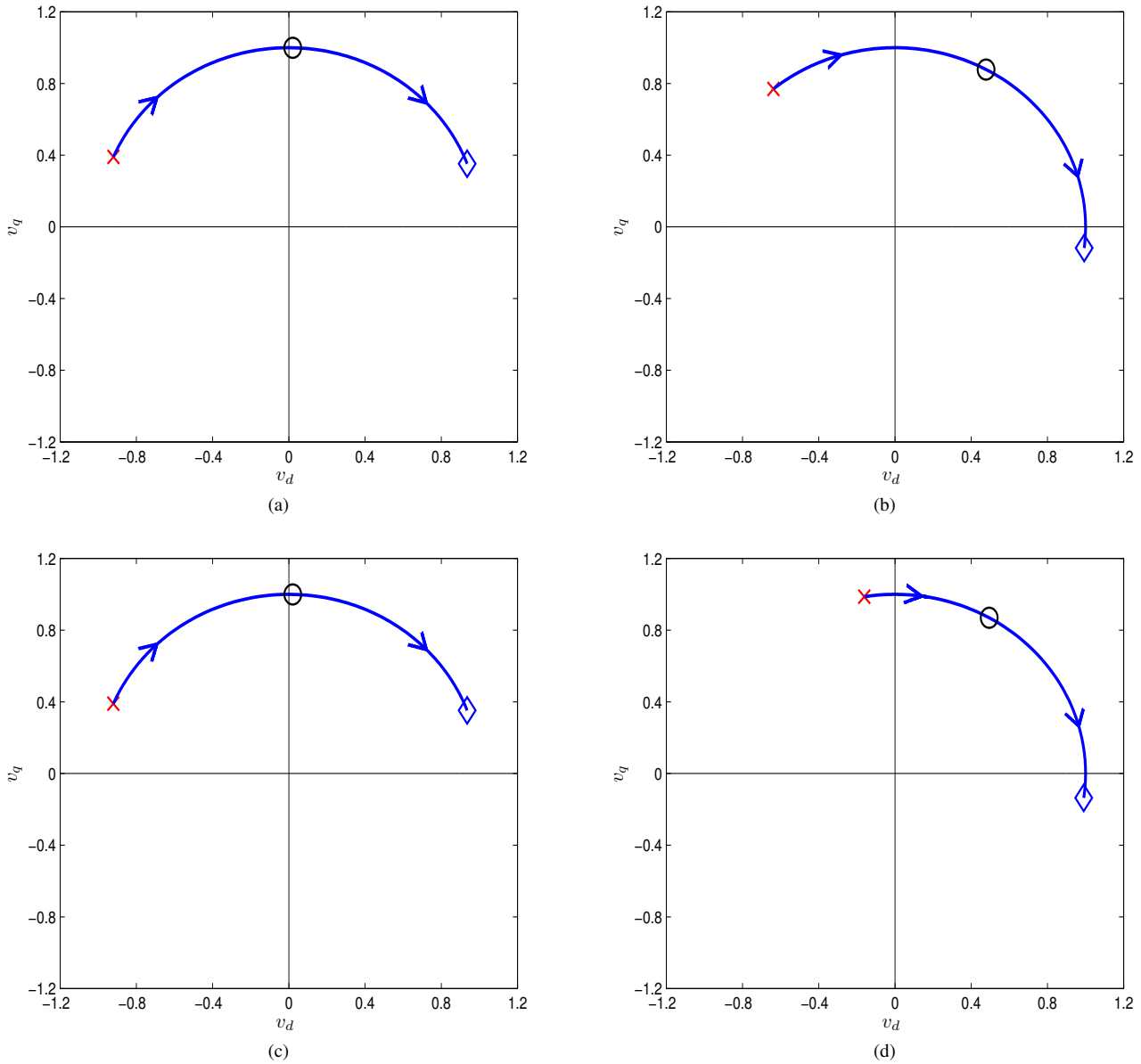

Fig. 4. Tracks of the normalized eigenvectors of the linearized system as i_q varies: (a) slow and (b) fast eigenvector for $\kappa = \sqrt{3}$, (c) slow and (d) fast eigenvector for κ selected according to (16). Crosses denote the starting points at $i_\mathrm{q} = -1$ p.u., circles denote the no-load points, and diamonds denote the end points at i_q = 1 p.u. Arrows denote the direction of increasing i_q, and are located at $|\beta|$ = 1.

The steady-state errors $\tilde{\psi}_{\mathrm{d}0}$ and $\tilde{R}_{\mathrm{s}0}$ can be obtained from

$$\tilde{\psi}_{\mathrm{d}0} = -\frac{1}{2} i_\mathrm{d} \left[(L_\mathrm{d} - L_\mathrm{q}) \cos(2\tilde{\vartheta}_{\mathrm{m}0}) + L_\mathrm{d} + L_\mathrm{q} - 2\hat{L}_\mathrm{d} \right] + \frac{1}{2} i_\mathrm{q} \sin(2\tilde{\vartheta}_{\mathrm{m}0})(L_\mathrm{d} - L_\mathrm{q}) \tag{21a}$$

$$\tilde{R}_{\mathrm{s}0} = \frac{L_\mathrm{d} + L_\mathrm{q} - 2\hat{L}_\mathrm{d} + (L_\mathrm{d} - L_\mathrm{q}) \cos(2\tilde{\vartheta}_{\mathrm{m}0})}{2\beta} \hat{\omega}_\mathrm{m} - \frac{(L_\mathrm{d} - L_\mathrm{q}) \sin(2\tilde{\vartheta}_{\mathrm{m}0})}{2} \hat{\omega}_\mathrm{m} \tag{21b}$$

It can be seen that the steady-state errors are independent of the gain selections, and only $\tilde{R}_{\mathrm{s}0}$ is affected by the estimated speed. Furthermore, $\tilde{R}_{\mathrm{s}0}$ increases as $\hat{\omega}_\mathrm{m}$ increases or β decreases, suggesting that the stator-resistance adaptation should be used only at low speeds and high load.

The estimation error dynamics are linearized in the vicinity of the steady-state error $\tilde{\vartheta}_{\mathrm{m}0}$, yielding

$$\frac{\mathrm{d}}{\mathrm{d}t} \begin{bmatrix} \tilde{\psi}_\mathrm{d} \\ \tilde{\psi}_\mathrm{q} \\ \tilde{R}_\mathrm{s} \end{bmatrix} = \begin{bmatrix} k_{10} & -k_{10}\beta' + \omega_{\mathrm{m}0} & -i_{\mathrm{d}0} \\ k_{20} - \omega_{\mathrm{m}0} & -k_{20}\beta' & -i_{\mathrm{q}0} \\ k_{\mathrm{R}0} & -k_{\mathrm{R}0}\beta' & 0 \end{bmatrix} \begin{bmatrix} \tilde{\psi}_\mathrm{d} \\ \tilde{\psi}_\mathrm{q} \\ \tilde{R}_\mathrm{s} \end{bmatrix} \tag{22}$$

These results can be used to optimize the stator-resistance adaptation gain $k_{\mathrm{R}0}$ in a fashion similar to optimization of the design parameters b and c. With accurate parameter estimates, the linearized system (22) is locally stable if the stability

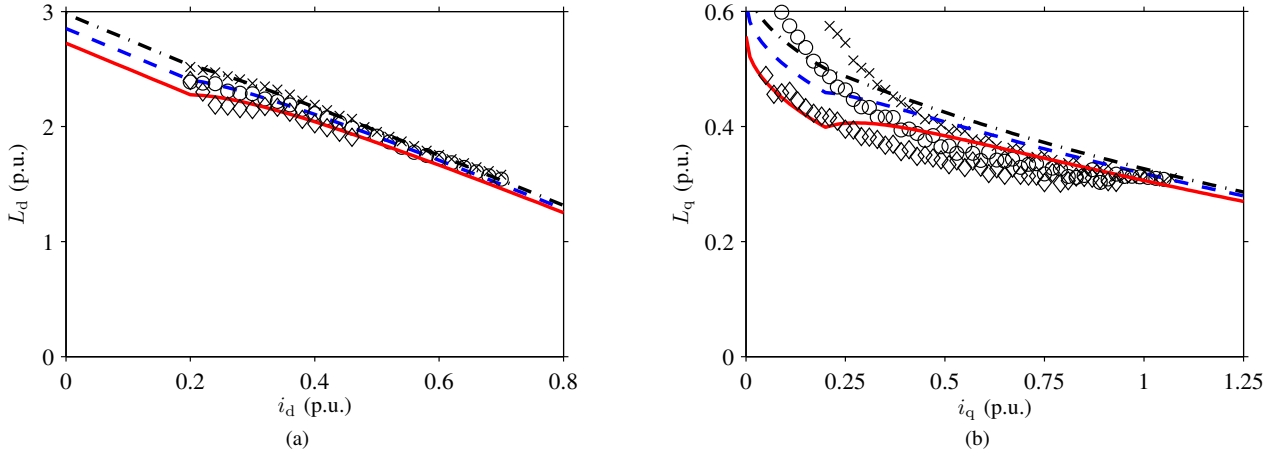

Fig. 5. Results of parameter estimation applied to the inductance values obtained from experimental data: (a) L_d as a function of i_d for three different values of i_q, (b) L_q as a function of i_q for three different values of i_d. In (a), the values of i_q are 0.4 p.u. (dash-dotted line), 0.7 p.u. (dashed line) and 1.0 p.u. (solid line). In (b), the values of i_d are 0.25 p.u. (dash-dotted line), 0.4 p.u. (dashed line) and 0.55 p.u. (solid line).

conditions (5) are satisfied.

IV. Experimental Setup and Parameters

The motion-sensorless control system was implemented in a dSPACE DS1104 PPC/DSP board. A 6.7-kW four-pole SyRM is fed by a frequency converter that is controlled by the DS1104 board. The rated values of the SyRM are: rotational speed 3175 r/min; frequency 105.8 Hz; line-to-line rms voltage 370 V; rms current 15.5 A; and torque 20.1 Nm. The base values for angular speed, voltage, and current are defined as $2\pi \cdot 105.8$ rad/s, $\sqrt{2/3} \cdot 370$ V, and $\sqrt{2} \cdot 15.5$ A, respectively.

A servo motor is used as a loading machine. The rotor speed ω_m and position ϑ_m are measured using an incremental encoder for monitoring purposes. The shaft torque is measured using a Dataflex 22 torque measuring shaft. The total moment of inertia of the experimental setup is 0.015 kgm^2 (2.7 times the inertia of the SyRM rotor).

The block diagram of the motion-sensorless control system implemented in the DS1104 board is shown in Fig. 1. The stator currents and the DC-link voltage are measured, and the reference voltage obtained from the current controller is used for the observer. The sampling is synchronized to the modulation, and both the switching frequency and the sampling frequency are 5 kHz. A simple current feedforward compensation for dead times and power device voltage drops is applied. The control system shown in Fig. 1 is augmented with a speed controller, whose feedback signal is the speed estimate $\hat{\omega}_\mathrm{m}$ obtained from the proposed observer. The bandwidth of this PI controller, including active damping [11], is $2\pi \cdot 5.3$ rad/s (0.05 p.u.). The stator-resistance adaptation is disabled in all experiments.

The saturation has been modeled as functions of the measured current,

$$L_\mathrm{d} = \begin{cases} L_\mathrm{d0} - \alpha i_\mathrm{d} - \delta \left| \frac{i_\mathrm{q}}{i_\mathrm{d0}} \right|, & \text{if } i_\mathrm{d} \le i_\mathrm{d0} \\ L_\mathrm{d0} - \alpha i_\mathrm{d} - \delta \left| \frac{i_\mathrm{q}}{i_\mathrm{d}} \right|, & \text{otherwise} \end{cases} \tag{23a}$$

$$L_\mathrm{q} = \begin{cases} L_\mathrm{q0} - \gamma \sqrt{|i_\mathrm{q}|} - \delta \left| \frac{i_\mathrm{d}}{i_\mathrm{q0}} \right|, & \text{if } i_\mathrm{q} \le i_\mathrm{q0} \\ L_\mathrm{q0} - \gamma \sqrt{|i_\mathrm{q}|} - \delta \left| \frac{i_\mathrm{d}}{i_\mathrm{q}} \right|, & \text{otherwise} \end{cases} \tag{23b}$$

where i_d0 and i_q0 are transition values for i_d and i_q to avoid divisions by small numbers. The measured inductances and the curves from the fitted functions are shown in Fig. 5. In Fig. 5(a), the d axis inductance L_d is shown as a function of i_d for three different values of i_q. In Fig. 5(b), L_q is shown as a function of i_q for three different values of i_d. The saturation model parameters are: $L_\mathrm{d0} = 3.15$ p.u., $L_\mathrm{q0} = 0.685$ p.u., $\alpha = 2.24$ p.u., $\gamma = 0.353$ p.u. and $\delta = 0.085$ p.u.

V. Experimental Results

Fig. 6 shows experimental results of a slow change of i_d from 0.3 p.u. to 0.5 p.u. at the speed $\hat{\omega}_\mathrm{m} = 0.1$ p.u. when the parameter $\kappa = \sqrt{3}$ and -50% of the rated load torque is applied. It can be seen that as i_d increases in the regenerating mode, the noise in the position estimate increases. This behavior suggests that the noise originates from saturation-induced harmonics. The frequency of the noise is approximately 21 Hz, which is two times the operating-point frequency (10.5 Hz), as can be seen in the magnification in Fig. 6(b).

Results of a stepwise speed reversal from $\hat{\omega}_\mathrm{m} = 0.10$ p.u. to $\hat{\omega}_\mathrm{m} = -0.10$ p.u. and back to 0.10 p.u. are depicted in Fig. 7. The rated load torque is applied, and $i_\mathrm{d} = 0.5$ p.u. It can be seen that the noise in the estimation error is amplified in the regenerating mode in Fig. 7(a), when $\kappa = \sqrt{3}$. With the selection (16) and $\kappa_\mathrm{min} = 0.6$, this noise is reduced in Fig. 7(b), as assumed based on the eigenvector analysis.

The effect of the parameter errors on the position estimation error at the speed $\hat{\omega}_\mathrm{m} = 0.1$ p.u. with 50% rated load torque

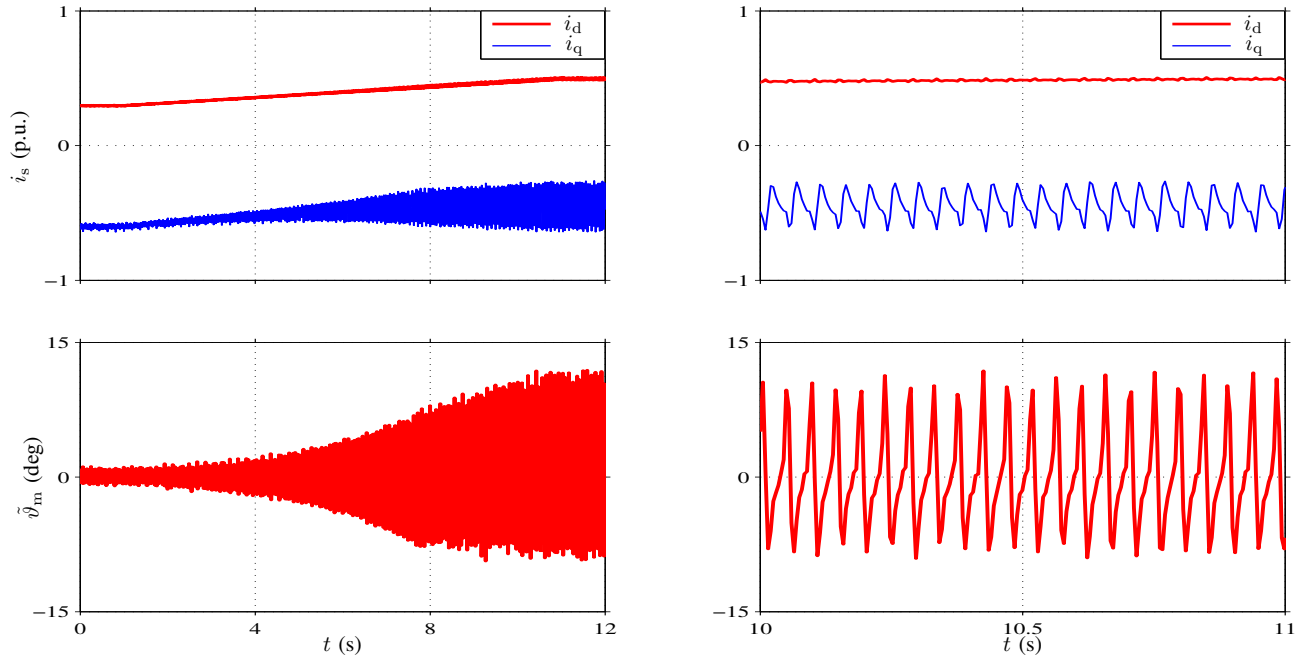

Fig. 6. Experimental results of a slow change in i_d from 0.3 p.u. to 0.5 p.u. with -50% of the rated load torque applied when $\kappa = \sqrt{3}$: (a) full sequence, (b) magnification from 10 s $\leq t \leq$ 11 s.

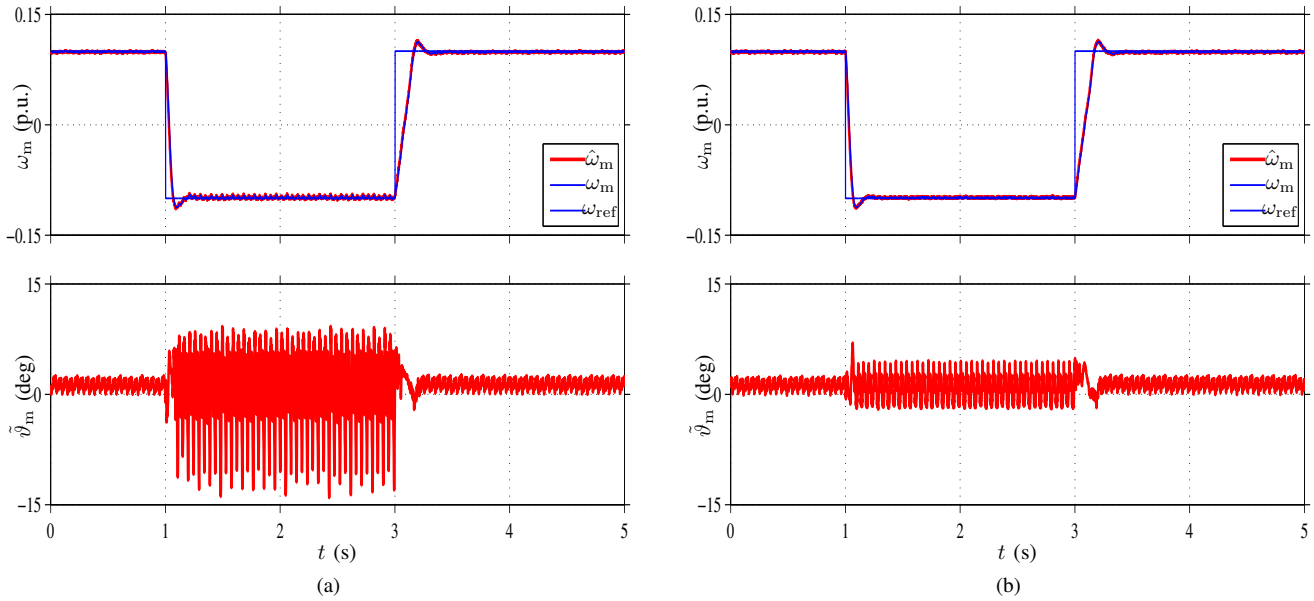

Fig. 7. Experimental results of a stepwise speed reversal (0.10 p.u. $\rightarrow -$ 0.10 p.u. $\rightarrow$ 0.10 p.u.) with rated load torque applied: (a) $\kappa = \sqrt{3}$, (b) κ is selected according to (16) and $\kappa_\mathrm{min} = 0.6$.

applied are shown in Fig. 8. The data is captured by disabling the saturation model and varying each model parameter from 90% up to 110% of the actual value in 10 seconds. It can be seen that the model parameters $\hat{R}_\mathrm{s}$ and $\hat{L}_\mathrm{q}$ have only a small effect on the position error, whereas an incorrect value for $\hat{L}_\mathrm{d}$ increases the estimation error rapidly. It should be noted that the relative errors of L_d and L_q are defined with respect to the (original) operating-point values. As the estimation error increases, the actual values of i_d and i_q change, resulting in changes in actual values of L_d and L_q due to saturation.

VI. Conclusions

In this paper, equations for steady-state errors and analytical stability conditions are derived for the reduced-order position observer with incorrect parameter estimates. Based on the stability conditions and small-signal dynamics, design rules

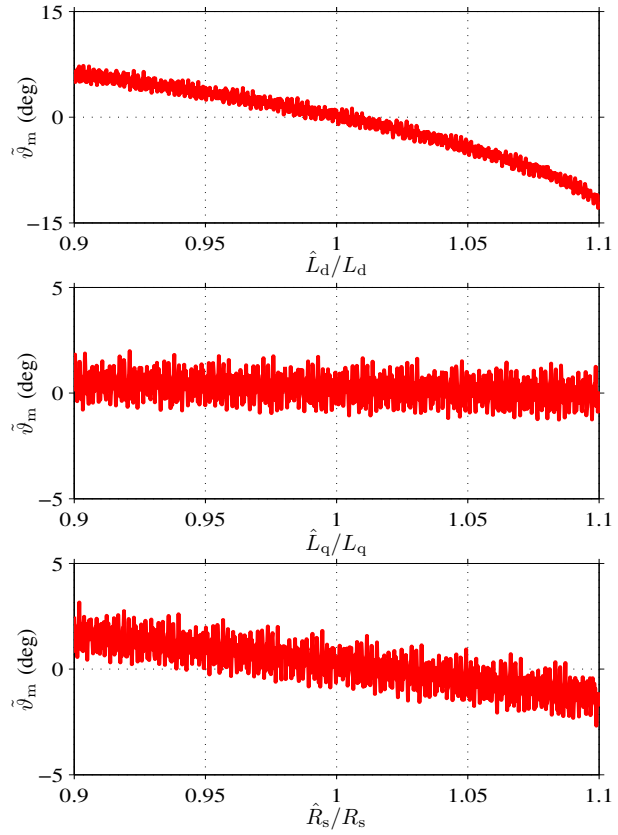

Fig. 8. Measured errors in the position estimate at $\hat{\omega}_\mathrm{m} = 0.1$ p.u. with 50% rated load torque applied. The data is captured by varying each model parameter from 90% up to 110% of the actual value in 10 seconds.

are proposed. The system can be augmented with the stator-resistance adaptation for improved low-speed operation. The equations for steady-state errors and small-signal dynamics are derived for the system augmented with the resistance adaptation. The performance of the proposed observer design was evaluated using laboratory experiments with a 6.7-kW SyRM drive. Stable operation at low speed under different parameter errors and different loads was demonstrated. With the proposed design rules, saturation-induced noise in the position estimate can be reduced.

ACKNOWLEDGMENT

The authors gratefully acknowledge ABB Oy for the financial support.

REFERENCES

[1] E. Capecchi, P. Guglielmo, M. Pastorelli, and A. Vagati, "Position-sensorless control of the transverse-laminated synchronous reluctance motor," *IEEE Trans. Ind. Appl.*, vol. 37, no. 6, pp. 1768–1776, Nov./Dec. 2001.

[2] H. F. Hofmann, S. R. Sanders, and A. EL-Antably, "Stator-flux-oriented vector control of synchronous reluctance machines with maximized efficiency," *IEEE Trans. Ind. Electron.*, vol. 51, no. 5, pp. 1066–1072, Oct. 2004.

[3] A. Piippo, M. Hinkkanen, and J. Luomi, "Sensorless control of PMSM drives using a combination of voltage model and HF signal injection," in *Conf. Rec. IEEE-IAS Annu. Meeting*, vol. 2, Seattle, WA, Oct. 2004, pp. 964–970.

[4] O. Wallmark, L. Harnefors, and O. Carlson, "An improved speed and position estimator for salient permanent-magnet synchronous motors," *IEEE Trans. Ind. Electron.*, vol. 52, no. 1, pp. 255–262, Feb. 2005.

[5] R. Lagerquist, I. Boldea, and J. Miller, "Sensorless control of the synchronous reluctance motor," *IEEE Trans. Ind. Appl.*, vol. 30, no. 3, pp. 673–682, 1994.

[6] T. Hanamoto, A. Ghaderi, M. Harada, and T. Tsuji, "Sensorless speed control of synchronous reluctance motor using a novel flux estimator based on recursive fourier transformation," in *Proceedings of the IEEE International Conference on Industrial Technology (ICIT '09)*, Churchill, Australia, Feb. 2009, pp. 1–6.

[7] S.-C. Agarlită, M. Fătu, L. N. Tutelea, F. Blaabjerg, and I. Boldea, "I-f starting and active flux based sensorless vector control of reluctance synchronous motors, with experiments," in *Proc. Optim'10*, vol. 1, Brasov, Romania, May 2010, pp. 337–342.

[8] J.-F. Stumper, D. Paulus, P. Landsmann, and R. Kennel, "Encoderless field-oriented control of a synchronous reluctance machine with a direct estimator," in *First Symposium on Sensorless Control for Electrical Drives (SLED), 2010*, Padova, Italy, July 2010, pp. 18–23.

[9] A. Vagati, M. Pastorelli, F. Scapino, and G. Franceschini, "Impact of cross saturation in synchronous reluctance motors of the trasverse-laminated type," *IEEE Trans. Ind. Appl.*, vol. 36, no. 4, pp. 1039–1046, Jul./Aug. 2000.

[10] M. Hinkkanen, T. Tuovinen, L. Harnefors, and J. Luomi, "A combined position and stator-resistance observer for salient PMSM drives: design and stability analysis," *IEEE Trans. Power Electron.*, vol. PP, no. 99, 2011, doi:10.1109/tpel.2011.2118232, in press.

[11] L. Harnefors, "Design and analysis of general rotor-flux-oriented vector control systems," *IEEE Trans. Ind. Electron.*, vol. 48, no. 2, pp. 383–390, Apr. 2001.